



# An active contour model and its algorithms with local and global Gaussian distribution fitting energies



Hui Wang<sup>a,b</sup>, Ting-Zhu Huang<sup>a,\*</sup>, Zongben Xu<sup>c</sup>, Yilun Wang<sup>a</sup>

<sup>a</sup> School of Mathematical Sciences/Institute of Computational Science, University of Electronic Science and Technology of China, Chengdu, Sichuan 611731, PR China

<sup>b</sup> Department of Mathematics and Computer Science, Anshun University, Anshun, Guizhou 561000, PR China

<sup>c</sup> Institute for Information and System Sciences, Xi'an Jiaotong University, Xi'an, Shan'xi 710049, PR China

## ARTICLE INFO

### Article history:

Received 8 September 2012

Received in revised form 6 March 2013

Accepted 28 October 2013

Available online 4 November 2013

### Keywords:

Active contour model

Image segmentation

Gaussian distribution

Level set method

Chan-Vese model

LBF model

## ABSTRACT

In this paper, we propose an active contour model and its corresponding algorithms with detailed implementation for image segmentation. In the proposed model, the local and global region fitting energies are described by the combination of the local and global Gaussian distributions with different means and variances, respectively. In this combination, we increase a weighting coefficient by which we can adjust the ratio between the local and global region fitting energies. Then we present an algorithm for implementing the proposed model directly. Considering that, in practice, the selection of the weighting coefficient is troublesome, we present a modified algorithm in order to overcome this problem and increase the flexibility. By adaptively updating the weighting coefficient and the time step with the contour evolution, this algorithm is less sensitive to the initialization of the contour and can speed up the convergence rate. Besides, it is robust to the noise and can be used to extract the desired objects. Experiment results demonstrate that the proposed model and its algorithms are effective with application to both the synthetic and real-world images.

© 2013 Elsevier Inc. All rights reserved.

## 1. Introduction

Image segmentation is always one of the major problems in image analysis and computer vision. In the past twenty years, numerous different approaches have been continuously proposed for handling this problem, such as those recent methods based on the fuzzy Dempster-Shafer inference system [16] and the feature space [36]. Due to the good performance, active contour models [8,9,12,19] based on the theory of curve and surface evolutions and geometric flows have been extensively studied and successfully used in the field of image segmentation. With explicit parametric curves, the original active contour model was introduced in [19] for extracting objects. As indicated there, this model has some intrinsic disadvantages, such as its difficulty in handling topological changes. In order to overcome this difficulty, level set method [29] which was firstly proposed by Osher and Sethian could effectively handle topological changes by representing curves or surfaces as the zero level set of a high dimensional function. Since the introduction of the level set method, it has become increasingly popular in many aspects of image processing and analysis. Furthermore, it is specially applied to develop active contour models for image segmentation.

Generally speaking, active contour models can be categorized into two different classes: edge-based models [9,15,30,39,43] and region-based models [12,20,22,23,34,35,38]. Edge-based models use the edge information to drive the active contour toward the object boundaries and stop there. This kind of models is sensitive to initial conditions and some-

\* Corresponding author. Tel.: +86 13688078826.

E-mail addresses: [wanghui561403@163.com](mailto:wanghui561403@163.com) (H. Wang), [tingzhuang@126.com](mailto:tingzhuang@126.com) (T.-Z. Huang).

times with some boundary leakage problems, especially to the weak or fuzzy boundaries. Compared with the edge-based models, region-based models do not rely on any edge and gradient information and are less sensitive to the noise and clutter. Moreover, the region-based models are usually less dependent on the initialization since they exploit the global region information of the image statistics. Therefore, in this paper, we mainly focus on the region-based models.

A large variety of region-based models and their related algorithms have been presented over the last twenty years and among them an increasingly prevalent kind of approaches is mainly concerned with the application of statistical methods [13]. These approaches are to define the data term usually by introducing statistical parametric models where each segmentation region is characterized by a set of parameters. In this way, it can distinguish the region from the others, such as the models based on Gaussian distribution [27,48], Gamma distribution [2], Weibull distribution [1], Wishart distribution [4], Rayleigh distribution [35] and Fisher-Tippett distribution [18]. These models are mainly stated by maximizing a likelihood estimation or maximizing a posteriori probability, which can be conditionally transformed to minimizing an equivalent energy functional. One of the most popular region-based models is Chan-Vese (C-V) model [12], which, as a special case of Mumford-Shah energy functional [28], is defined by minimizing an energy functional to approximate the image in piecewise constant forms. On the basis of the C-V model, in [6,7,10], the authors further present and develop a series of global minimization methods. However, the C-V model is always based on the assumption that the image is statistically intensity homogeneous in each region so that it exists some limitations in practical applications. In fact, intensity inhomogeneous images widely exist in the real world, such as medical imaging due to some technical limitations or artificial factors. As a whole, intensity inhomogeneity is still considered as a challenging problem in image segmentation. Based on the single level set model, a multiphase level set framework [40] is presented for the multi-region image segmentation, which can be used to deal with the problem of intensity inhomogeneity. However, it requires periodical reinitialization of the level set function so that the computational cost is expensive. And especially for the image with severe intensity inhomogeneity, the effectiveness is unsatisfactory. Later on, local region information has been incorporated into the active contour models and it is worth mentioning that local binary fitting (LBF) model [22,23], also called region-scalable fitting model, performs better than the C-V model on extracting objects for the image with intensity inhomogeneity. But the LBF model is sensitive to the initialization of the contour. And especially if the initial position of the contour is far away from the object boundaries, the LBF model may be prone to getting stuck in local minima.

In practice, how to effectively integrate the advantages of the local and global region information plays an important role in improving the segmentation quality. Apart from the LBF model, in [21,41,45], active contour models mainly based on the local region information are further developed in various ways, which are effective to the image with intensity inhomogeneity. In [5,42], on the basis of complementary advantages, the local and global region information are incorporated with each other to increase the flexibility and obtain more desirable results. On the other hand, based on the consideration of image information and application, a major concern is to obtain the selective objects [3,32,46], which has some positive significance particularly with application to medical imaging in order to extract the partial desired objects for helping medical diagnosis.

Among the region-based models, in the following we pay attention to the introduction of statistic methods. For simplicity, let  $I: \mathbf{x} \in \Omega \rightarrow R$  be a given image, where  $\mathbf{x}$  is a vector to represent a point in the domain  $\Omega$ . Similarly to [13,31,35], we assume that the intensity of each point is a random variable and its pixel intensity in each local region is independent and identically distributed. Without loss of generality, we consider a two-region image segmentation problem based on the statistical methods. Generally the problem of maximizing likelihood estimation or maximizing a posterior probability based on probability density functions is equivalent to minimizing an energy functional with their negative logarithm forms expressed as follows:

$$E(I(\mathbf{x}), C) = - \int_{\Omega_1} \log p(I(\mathbf{x}); \Omega_1) d\mathbf{x} - \int_{\Omega_2} \log p(I(\mathbf{x}); \Omega_2) d\mathbf{x}, \quad (1)$$

where  $\Omega_1$  and  $\Omega_2$  represent inside and outside regions of the contour  $C$ , respectively.

In this paper, based on the merits of the local and global region fitting energies, such as the LBF model and the C-V model, respectively, we firstly propose an active contour model. In this proposed model, the local and global region fitting energies are described by a combination of the local and global Gaussian distributions with different means and variances, respectively. In this combination of the proposed model, we increase a weighting coefficient by which we can dynamically adjust the ratio between the local and global region fitting energies. Subsequently, we introduce the level set method to realize the contour evolution and deduce the corresponding gradient descent flow equation, which can be easily implemented by the finite difference method. Secondly, we present an algorithm for implementing the proposed model directly. Nevertheless, in practice, the selection of the weighting coefficient is not an easy task. If we set a large weight coefficient, we cannot effectively deal with the image with intensity inhomogeneity. On the contrary, if we set it to be small, the proposed model is with slow convergence and sensitive to the initialization of the contour. In summary, the selection of a suitable weighting coefficient needs a large number of trials and modifications and the process is time-consuming. To overcome this problem, we further present a modified algorithm in which the weighting coefficient and the time step of the iteration can be adaptively updated with the contour evolution. That is to say, we can obtain an adaptive weighting coefficient and a fit time step, which are helpful to detect the object boundaries and speed up the convergence rate. More specifically, for the convenience of the initialization of the contour, sometimes we can set a relatively large weight coefficient at the beginning. And then when the

contour goes near the object boundaries, we reduce the weighting coefficient gradually. Meanwhile, if it is necessary, we decrease the time step for the benefit of detecting the object boundaries accurately. Therefore, this algorithm is effective and fit to the image with intensity inhomogeneity. In addition, it is insensitive to the noise and can be specially used to detect the desired objects.

The rest of this paper is organized as follows. In Section 2, we mainly review the popular C-V model and the LBF model. In Section 3, we propose a new active contour model and its corresponding algorithms. In Section 4, we carry out some experiments to demonstrate the effectiveness and performance of our algorithms. Finally, we summarize this paper in Section 5.

## 2. Background

In the region-based active contour models, the local or global region information is usually employed to define the image fitting energy functional. In this section, in order to make preparation for the introduction of the proposed model, we first briefly review the popular C-V model and the LBF model as two kinds of typical examples based on the global and local region fitting energies, respectively.

### 2.1. The C-V model

In [12], by simplifying the Mumford-Shah functional [28], Chan and Vese introduced the contour  $C$  to divide the image into inside and outside regions which are expressed as  $in(C)$  and  $out(C)$ , respectively. They used two constants  $c_1$  and  $c_2$  to approximate the image intensities of every region. The energy functional of the C-V model is defined as follows:

$$E(C, c_1, c_2) = \mu \cdot \text{Length}(C) + \nu \cdot \text{Area}(\text{inside}(C)) + \lambda_1 \int_{in(C)} |I(\mathbf{x}) - c_1|^2 d\mathbf{x} + \lambda_2 \int_{out(C)} |I(\mathbf{x}) - c_2|^2 d\mathbf{x}, \quad (2)$$

where  $\mu \geq 0$ ,  $\nu \geq 0$ ,  $\lambda_1 > 0$ ,  $\lambda_2 > 0$  are parameters.

The first term of the energy functional (2) is the length restraint term of the contour and the second term is the area restraint term of the inside region. The last two terms, called fitting energy based on the inside and outside regions of the contour, play a major role in the process of the contour evolution. In calculus of variations, by minimizing the energy functional (2) with respect to the level set function  $\phi$ , the corresponding level set formulation is obtained as follows:

$$\frac{\partial \phi}{\partial t} = \delta(\phi) \left[ \mu \text{div} \left( \frac{\nabla \phi}{|\nabla \phi|} \right) - \nu - \lambda_1 (I(\mathbf{x}) - c_1)^2 + \lambda_2 (I(\mathbf{x}) - c_2)^2 \right], \quad (3)$$

where  $\text{div}(\cdot)$  is the divergence operator and  $\delta$  is the Dirac function. Similarly,  $c_1$  and  $c_2$  are obtained by

$$c_1(\phi) = \frac{\int I(\mathbf{x}) H(\phi(\mathbf{x})) d\mathbf{x}}{\int H(\phi(\mathbf{x})) d\mathbf{x}}, \quad (4)$$

$$c_2(\phi) = \frac{\int I(\mathbf{x}) (1 - H(\phi(\mathbf{x}))) d\mathbf{x}}{\int (1 - H(\phi(\mathbf{x}))) d\mathbf{x}}, \quad (5)$$

where  $H$  is the Heaviside function.

The C-V model, based on techniques of curve evolution and the level set method, is considered as one of the most widely used models for two-region image segmentation. However, what is limited is that, the C-V model always supposes the image with intensity homogeneity. In fact, from Eqs. (4) and (5) we can observe that  $c_1$  and  $c_2$  are mainly related to the global properties for they rely on the region information inside and outside the contour, respectively. Because it does not take the local image information into account, the C-V model cannot effectively segment the image with intensity inhomogeneity.

### 2.2. The LBF model

In image segmentation, the LBF model [22,23] was primarily proposed for exploiting the local region information to deal with the problem of intensity inhomogeneity. Its energy functional is defined as follows:

$$E(C, f_1(\mathbf{x}), f_2(\mathbf{x})) = \lambda_1 \int \left[ \int_{in(C)} K_\sigma(\mathbf{x} - \mathbf{y}) |I(\mathbf{y}) - f_1(\mathbf{x})|^2 d\mathbf{y} \right] d\mathbf{x} + \lambda_2 \int \left[ \int_{out(C)} K_\sigma(\mathbf{x} - \mathbf{y}) |I(\mathbf{y}) - f_2(\mathbf{x})|^2 d\mathbf{y} \right] d\mathbf{x}, \quad (6)$$

where  $\lambda_1$  and  $\lambda_2$  are positive constants.

In the energy functional (6),  $f_1(\mathbf{x})$  and  $f_2(\mathbf{x})$  are two smooth functions that are used to locally approximate image intensities inside and outside the contour, respectively, and  $K_\sigma$  is a Gaussian kernel function with standard deviation  $\sigma$  defined by

$$K_\sigma(\mathbf{x} - \mathbf{y}) = \frac{1}{(2\pi)^{n/2} \sigma^n} \exp \left( -\frac{|\mathbf{x} - \mathbf{y}|^2}{2\sigma^2} \right). \quad (7)$$

In the LBF model, for each center point  $\mathbf{x}$ , the values of  $f_1(\mathbf{x})$  and  $f_2(\mathbf{x})$  only fit the image intensities in a local region near  $\mathbf{x}$  because of the effect of the Gaussian kernel function  $K_\sigma(\mathbf{x} - \mathbf{y})$ . If  $\mathbf{y}$  is near  $\mathbf{x}$ , the value of  $K_\sigma(\mathbf{x} - \mathbf{y})$  is large and the contribution of the intensity  $I(\mathbf{y})$  to the energy functional is significant. On the contrary, when  $\mathbf{y}$  goes away from  $\mathbf{x}$ ,  $K_\sigma(\mathbf{x} - \mathbf{y})$  decreases drastically to zero so that the contribution of the intensity  $I(\mathbf{y})$  to the energy functional approaches to zero. In fact,  $f_1(\mathbf{x})$  and  $f_2(\mathbf{x})$  can be considered as the local weighting averages of the image intensities in the Gaussian window inside and outside the contour, respectively. In some sense, these local averages are more effective than the global averages  $c_1$  and  $c_2$  shown in the C-V model.

Due to the introduction of the kernel function, and the utilization of the local region fitting energy of the image, the LBF model can cope with the intensity inhomogeneity well. However, the local region information is not always enough for effective and accurate image segmentation. Furthermore, the LBF model depends on the initialization of the contour. And in particular, if we set the initial position of the contour far away from the object boundaries, the LBF model is prone to getting stuck in local minima.

### 3. An active contour model and its algorithms

Notice that the local or global region information alone is not enough for image segmentation. Hence, in consideration of their respective merits and limitations, we will consider to propose an active contour model with both the local and global Gaussian distribution fitting energies and further present its algorithms for implementation in this section.

#### 3.1. An active contour model with local and global Gaussian distribution fitting energies

As stated in Section 2, the C-V model and the LBF model have their respective advantages and disadvantages, because the former is mainly based on the global region information and to the latter, the local region information is pivotal. Hence, with a view to finding more applicable methods, it is natural and meaningful to consider integrating their merits. In image segmentation, whether the object boundaries and the fine structures can be accurately detected largely depends on the local neighbor region information. Meanwhile, to reduce the impact of the noise and the possibility of getting stuck in local minima, the global region information plays a leading role. Particularly it is crucial to decrease the sensitivity to the initialization of the contour. In fact, the local and global region fitting energies are based on the local and global region information of the image, respectively. Motivated by the contributions and methods in [21,41,48], and the works of the LBF model [22,23], we propose an active contour model for incorporating the local and global region information of the image. From a statistical point of view, in the proposed model, the fitting energy is described by a combination of the local and global Gaussian distributions with different means and variances, respectively. Firstly, by increasing the length of the contour as a restraint term as shown in [12], we define an energy functional as follows:

$$\begin{aligned} E(C, u_1(\mathbf{x}), u_2(\mathbf{x}), \sigma_1^2(\mathbf{x}), \sigma_2^2(\mathbf{x}), u_3, u_4, \sigma_3^2, \sigma_4^2) = & \nu \cdot \text{length}(C) - (1 - \theta) \left\{ \int \left[ \int_{\Omega_1} K_\sigma(\mathbf{x} - \mathbf{y}) \log p_{1,\mathbf{x}}(I(\mathbf{y}), u_1(\mathbf{x}), \sigma_1^2(\mathbf{x})) d\mathbf{y} \right] d\mathbf{x} \right. \\ & + \left. \int \left[ \int_{\Omega_2} K_\sigma(\mathbf{x} - \mathbf{y}) \log p_{2,\mathbf{x}}(I(\mathbf{y}), u_2(\mathbf{x}), \sigma_2^2(\mathbf{x})) d\mathbf{y} \right] d\mathbf{x} \right\} \\ & - \theta \left\{ \int_{\Omega_1} \log p_3(I(\mathbf{x}), u_3, \sigma_3^2) d\mathbf{x} + \int_{\Omega_2} \log p_4(I(\mathbf{x}), u_4, \sigma_4^2) d\mathbf{x} \right\}, \end{aligned} \quad (8)$$

where  $\nu$  and  $\theta$  are nonnegative constants.

In the energy functional (8), the first term is the length restraint term, and the second and third terms are the local and global region fitting energies, respectively. Here, we still focus on two regions:  $\Omega_1 = \text{in}(C)$ ,  $\Omega_2 = \text{out}(C)$ .  $K_\sigma$  is a Gaussian kernel function defined as (7) in the LBF model and its role is similar to a window function.  $u_1(\mathbf{x})$  and  $u_2(\mathbf{x})$  are two functions in the variable  $\mathbf{x}$ , which are respectively used to approximate the local mean intensities of the neighbor region of the point  $\mathbf{x}$  inside and outside the contour  $C$ . Similarly,  $\sigma_1^2(\mathbf{x})$  and  $\sigma_2^2(\mathbf{x})$  approximate the local variances of the neighbor region intensities of the point  $\mathbf{x}$  inside and outside the contour  $C$ . Besides, different from the former description,  $u_3$  and  $u_4$  represent global mean intensities inside and outside the contour  $C$ . Analogously,  $\sigma_3^2$  and  $\sigma_4^2$  represent global variances of intensities inside and outside the contour  $C$ .  $p_{1,\mathbf{x}}(I(\mathbf{y}), u_1(\mathbf{x}), \sigma_1^2(\mathbf{x}))$  and  $p_{2,\mathbf{x}}(I(\mathbf{y}), u_2(\mathbf{x}), \sigma_2^2(\mathbf{x}))$  are probability density functions of local region intensities defined as the Gaussian distributions

$$p_{i,\mathbf{x}}(I(\mathbf{y}), u_i(\mathbf{x}), \sigma_i^2(\mathbf{x})) = \frac{1}{\sqrt{2\pi}\sigma_i(\mathbf{x})} \exp\left(-\frac{(I(\mathbf{y}) - u_i(\mathbf{x}))^2}{2\sigma_i^2(\mathbf{x})}\right), \quad (9)$$

where  $i = 1, 2$ , correspond to the inside and outside regions of the contour  $C$ . On the other hand,  $p_3(I(\mathbf{x}), u_3, \sigma_3^2)$  and  $p_4(I(\mathbf{x}), u_4, \sigma_4^2)$  are probability density functions of global region intensities defined as

$$p_j(I(\mathbf{x}), u_j, \sigma_j^2) = \frac{1}{\sqrt{2\pi}\sigma_j} \exp\left(-\frac{(I(\mathbf{x}) - u_j)^2}{2\sigma_j^2}\right), \quad (10)$$

where  $j = 3, 4$ , correspond to the inside and outside regions of the contour  $C$ . To be simple, we call Eqs. (9) as local probability density functions and Eq. (10) as global probability density functions. Besides, we call  $u_1(\mathbf{x})$  and  $u_2(\mathbf{x})$  as local means,  $\sigma_1^2(\mathbf{x})$  and  $\sigma_2^2(\mathbf{x})$  as local variances,  $u_3$  and  $u_4$  as global means,  $\sigma_3^2$  and  $\sigma_4^2$  as global variances. Therefore, the combination of the second and third terms in the energy functional (8) is called local and global Gaussian distribution fitting energies.

Further considering the expression of the energy functional (8), we set  $0 \leq \theta \leq 1$  and call it as a weighting coefficient in the following, by which we can adjust the ratio between the local and global region fitting energies. In fact, if  $\theta = 1$ , the energy functional is fully based on the global region fitting energy. On the other hand, if  $\theta = 0$ , the energy functional completely relies on the local region fitting energy.

According to the introduction of the level set function  $\phi$ , we assume  $\Omega_1 = \{\phi > 0\}$  and  $\Omega_2 = \{\phi < 0\}$ . Correspondingly, the contour  $C$  is expressed by the zero level set as  $C = \{\phi = 0\}$ . As can be seen in [12], we introduce the Heaviside function  $H$  and the Dirac function  $\delta$ , and then the energy functional (8) is rewritten as follows:

$$\begin{aligned} & E(\phi, u_1(\mathbf{x}), u_2(\mathbf{x}), \sigma_1^2(\mathbf{x}), \sigma_2^2(\mathbf{x}), u_3, u_4, \sigma_3^2, \sigma_4^2) \\ &= v \int |\nabla H(\phi(\mathbf{x}))| d\mathbf{x} + (1 - \theta) \left\{ \int \left[ \int K_\sigma(\mathbf{x} - \mathbf{y}) \left( \log \sqrt{2\pi} + \log \sigma_1(\mathbf{x}) + \frac{(I(\mathbf{y}) - u_1(\mathbf{x}))^2}{2\sigma_1^2(\mathbf{x})} \right) H(\phi(\mathbf{y})) d\mathbf{y} \right] d\mathbf{x} \right. \\ & \quad \left. + \int \left[ \int K_\sigma(\mathbf{x} - \mathbf{y}) \left( \log \sqrt{2\pi} + \log \sigma_2(\mathbf{x}) + \frac{(I(\mathbf{y}) - u_2(\mathbf{x}))^2}{2\sigma_2^2(\mathbf{x})} \right) (1 - H(\phi(\mathbf{y}))) d\mathbf{y} \right] d\mathbf{x} \right\} \\ & \quad + \theta \left\{ \int \left( \log \sqrt{2\pi} + \log \sigma_3 + \frac{(I(\mathbf{x}) - u_3)^2}{2\sigma_3^2} \right) H(\phi(\mathbf{x})) d\mathbf{x} + \int \left( \log \sqrt{2\pi} + \log \sigma_4 + \frac{(I(\mathbf{x}) - u_4)^2}{2\sigma_4^2} \right) (1 - H(\phi(\mathbf{x}))) d\mathbf{x} \right\}, \end{aligned} \quad (11)$$

where  $\sigma_i(\mathbf{x}) (i = 1, 2)$  are called local standard deviations, and similarly  $\sigma_j (j = 3, 4)$  are called global standard deviations.

With the level set evolution, usually it may become too steep or flat, which is unfavorable for numerical stability. Therefore, it is necessary to reinitialize the level set function for maintaining the signed distance property [14,17,24,37]. In order to preserve the level set function regularity and eliminate the reinitialization, we introduce a general distance regularized level set evolution (DRLSE) [25] energy term proposed by Li et al. as follows:

$$R_p(\phi) = \int p(|\nabla \phi(\mathbf{x})|) d\mathbf{x}, \quad (12)$$

where  $p$  is called a double-well potential function defined by

$$p(z) = \begin{cases} \frac{1}{(2\pi)^2} (1 - \cos(2\pi z)), & \text{if } z < 1, \\ \frac{1}{2} (z - 1)^2, & \text{if } z \geq 1. \end{cases} \quad (13)$$

Consequently, the total energy functional of this paper is expressed as follows:

$$F(\phi, u_1(\mathbf{x}), u_2(\mathbf{x}), \sigma_1^2(\mathbf{x}), \sigma_2^2(\mathbf{x}), u_3, u_4, \sigma_3^2, \sigma_4^2) = \mu R_p(\phi) + E(\phi, u_1(\mathbf{x}), u_2(\mathbf{x}), \sigma_1^2(\mathbf{x}), \sigma_2^2(\mathbf{x}), u_3, u_4, \sigma_3^2, \sigma_4^2), \quad (14)$$

where  $\mu$  is a positive constant. Depending on the expression of the Gaussian distribution, the total energy functional incorporates the local and global region information of the image via the introduction of the weighting coefficient. Besides, owing to the introduction of DRLSE, we eliminate the complex reinitialization procedure of traditional level set methods.

In practice, as mentioned in [12,23], usually the Heaviside function  $H$  and the Dirac function  $\delta$  are respectively approximated by a smooth function  $H_\varepsilon$  and its derivative  $\delta_\varepsilon$  defined by

$$H_\varepsilon(z) = \frac{1}{2} \left[ 1 + \frac{2}{\pi} \arctan \left( \frac{z}{\varepsilon} \right) \right],$$

and

$$\delta_\varepsilon(z) = \frac{1}{\pi} \frac{\varepsilon}{\varepsilon^2 + z^2}.$$

Therefore, the total energy functional (14) can be approximated as follows:

$$F_\varepsilon(\phi, u_1(\mathbf{x}), u_2(\mathbf{x}), \sigma_1^2(\mathbf{x}), \sigma_2^2(\mathbf{x}), u_3, u_4, \sigma_3^2, \sigma_4^2) = \mu R_p(\phi) + E_\varepsilon(\phi, u_1(\mathbf{x}), u_2(\mathbf{x}), \sigma_1^2(\mathbf{x}), \sigma_2^2(\mathbf{x}), u_3, u_4, \sigma_3^2, \sigma_4^2). \quad (15)$$

By using the standard gradient descent method, at first, we fix  $\phi$  and minimize the energy functional (15) with respect to other variables alternately. Then we obtain the local means and variances as follows:

$$u_1(\mathbf{x}) = \frac{\int K_\sigma(\mathbf{x} - \mathbf{y}) I(\mathbf{y}) H_\varepsilon(\phi(\mathbf{y})) d\mathbf{y}}{\int K_\sigma(\mathbf{x} - \mathbf{y}) H_\varepsilon(\phi(\mathbf{y})) d\mathbf{y}}, \quad (16)$$

$$u_2(\mathbf{x}) = \frac{\int K_\sigma(\mathbf{x} - \mathbf{y}) I(\mathbf{y}) (1 - H_\varepsilon(\phi(\mathbf{y}))) d\mathbf{y}}{\int K_\sigma(\mathbf{x} - \mathbf{y}) (1 - H_\varepsilon(\phi(\mathbf{y}))) d\mathbf{y}}, \quad (17)$$

$$\sigma_1^2(\mathbf{x}) = \frac{\int K_\sigma(\mathbf{x} - \mathbf{y}) (I(\mathbf{y}) - u_1(\mathbf{x}))^2 H_\varepsilon(\phi(\mathbf{y})) d\mathbf{y}}{\int K_\sigma(\mathbf{x} - \mathbf{y}) H_\varepsilon(\phi(\mathbf{y})) d\mathbf{y}}, \quad (18)$$

$$\sigma_2^2(\mathbf{x}) = \frac{\int K_\sigma(\mathbf{x} - \mathbf{y}) (I(\mathbf{y}) - u_2(\mathbf{x}))^2 (1 - H_\varepsilon(\phi(\mathbf{y}))) d\mathbf{y}}{\int K_\sigma(\mathbf{x} - \mathbf{y}) (1 - H_\varepsilon(\phi(\mathbf{y}))) d\mathbf{y}}, \quad (19)$$

and the global means and variances as follows:

$$u_3 = \frac{\int I(\mathbf{x})H_e(\phi(\mathbf{x}))d\mathbf{x}}{\int H_e(\phi(\mathbf{x}))d\mathbf{x}}, \quad (20)$$

$$u_4 = \frac{\int I(\mathbf{x})(1 - H_e(\phi(\mathbf{x})))d\mathbf{x}}{\int (1 - H_e(\phi(\mathbf{x})))d\mathbf{x}}, \quad (21)$$

$$\sigma_3^2 = \frac{\int (I(\mathbf{x}) - u_3)^2 H_e(\phi(\mathbf{x}))d\mathbf{x}}{\int H_e(\phi(\mathbf{x}))d\mathbf{x}}, \quad (22)$$

$$\sigma_4^2 = \frac{\int (I(\mathbf{x}) - u_4)^2 (1 - H_e(\phi(\mathbf{x})))d\mathbf{x}}{\int (1 - H_e(\phi(\mathbf{x})))d\mathbf{x}}. \quad (23)$$

Subsequently, we keep all the variables fixed except for  $\phi$ , then minimizing the total energy functional (15) with respect to  $\phi$  is equivalent to solving the gradient descent flow equation as follows:

$$\frac{\partial \phi}{\partial t} = \mu \operatorname{div}(d_p(|\nabla \phi|)\nabla \phi) + v\delta_e(\phi)\operatorname{div}\left(\frac{\nabla \phi}{|\nabla \phi|}\right) - \delta_e(\phi)[(1 - \theta)(e_1 - e_2) + \theta(e_3 - e_4)], \quad (24)$$

where  $d_p(z)$  is defined by

$$d_p(z) = \frac{p'(z)}{z}.$$

In addition,  $e_1, e_2$  are given by

$$e_i = \int K_\sigma(\mathbf{y} - \mathbf{x}) \left( \log \sigma_i(\mathbf{y}) + \frac{(I(\mathbf{x}) - u_i(\mathbf{y}))^2}{2\sigma_i^2(\mathbf{y})} \right) d\mathbf{y}, \quad i = 1, 2, \quad (25)$$

and  $e_3, e_4$  are given by

$$e_j = \log \sigma_j + \frac{(I(\mathbf{x}) - u_j)^2}{2\sigma_j^2}, \quad j = 3, 4. \quad (26)$$

In the level set formulation (24), our analysis mainly focuses on the right-hand side. The first term  $\mu \operatorname{div}(d_p(|\nabla \phi|)\nabla \phi)$  derived from DRLSE is used to maintain the regularity of the level set function. In particular, the parameter  $\mu$  controls the weight of regularization and it should be relatively small as stated in [25]. The middle term  $v\delta_e(\phi)\operatorname{div}(\frac{\nabla \phi}{|\nabla \phi|})$  is the length-restraint term of the contour  $C$ . The last term  $-\delta_e(\phi)[(1 - \theta)(e_1 - e_2) + \theta(e_3 - e_4)]$  originated from the local and global region fitting energies plays a dominant role in the total energy functional.

**Remark 1.** In the proposed model (8) or (11), we have not simply integrated or combined the C-V model and the LBF model. Considering the problem from another perspective, we employ the Gaussian distribution to design the local and global fitting energies. If  $\theta = 1$ ,  $\sigma_3^2 = \sigma_4^2 = 0.5$ , and  $\sigma \rightarrow \infty$ , the proposed model will degenerate to the C-V model. If  $\theta = 0$ ,  $\sigma_1^2(\mathbf{x}) = \sigma_2^2(\mathbf{x}) = 0.5$ , the proposed model will be the same as the LBF model.

### 3.2. Algorithms and numerical approximation

In the proposed model, the contour is driven by the local and global region fitting energies, both of which are complementary to each other. When the contour is in the neighbor region of the object boundaries, the local region fitting energy plays a dominant role to control the movement and stop of the contour. On the other hand, when the contour is far away from the object boundaries, the global region fitting energy has a decisive effect on the contour evolution.

As noted in Section 3.1,  $\theta$  is considered as the weighting coefficient of the local and global region fitting energies. Clearly, once the value of  $\theta$  is set, simultaneously  $1 - \theta$  is also determined. In terms of application to the image with severe intensity inhomogeneity, we should choose a relatively small  $\theta$ . At this time,  $1 - \theta$  is relatively large, which means that the contour evolution is mainly driven by the local region fitting energy. By contrast, if the intensity inhomogeneity is low, a relatively large  $\theta$  should be set so as to make the global region fitting energy be dominant for the convenience of initializing the contour and speeding up the convergence rate. Therefore, in practical applications, it is very requisite to choose a suitable  $\theta$  for obtaining preferable segmentation results.

For solving the level set formulation (24), we first need to calculate the local means  $u_1(\mathbf{x}), u_2(\mathbf{x})$ , variances  $\sigma_1^2(\mathbf{x}), \sigma_2^2(\mathbf{x})$ ,  $e_1$  and  $e_2$ . More specifically, the calculations of  $u_1(\mathbf{x})$  and  $u_2(\mathbf{x})$  are described in details as follows:

$$u_1(\mathbf{x}) = \frac{K_\sigma(\mathbf{x}) * [I(\mathbf{x})H_e(\phi(\mathbf{x}))]}{K_\sigma(\mathbf{x}) * H_e(\phi(\mathbf{x}))},$$

$$u_2(\mathbf{x}) = \frac{K_\sigma(\mathbf{x}) * [I(\mathbf{x})(1 - H_e(\phi(\mathbf{x})))]}{K_\sigma(\mathbf{x}) * (1 - H_e(\phi(\mathbf{x})))}.$$



And the calculations of  $\sigma_1^2(\mathbf{x})$  and  $\sigma_2^2(\mathbf{x})$  are described by

$$\begin{aligned}\sigma_1^2(\mathbf{x}) &= \frac{\int K_\sigma(\mathbf{x} - \mathbf{y})(I(\mathbf{y}) - u_1(\mathbf{x}))^2 H_\varepsilon(\phi(\mathbf{y})) d\mathbf{y}}{\int K_\sigma(\mathbf{x} - \mathbf{y}) H_\varepsilon(\phi(\mathbf{y})) d\mathbf{y}} \\ &= \frac{\int K_\sigma(\mathbf{x} - \mathbf{y}) [I^2(\mathbf{y}) H_\varepsilon(\phi(\mathbf{y}))] d\mathbf{y}}{\int K_\sigma(\mathbf{x} - \mathbf{y}) H_\varepsilon(\phi(\mathbf{y})) d\mathbf{y}} - \frac{2u_1(\mathbf{x}) \int K_\sigma(\mathbf{x} - \mathbf{y}) [I(\mathbf{y}) H_\varepsilon(\phi(\mathbf{y}))] d\mathbf{y}}{\int K_\sigma(\mathbf{x} - \mathbf{y}) H_\varepsilon(\phi(\mathbf{y})) d\mathbf{y}} + \frac{u_1^2(\mathbf{x}) \int K_\sigma(\mathbf{x} - \mathbf{y}) H_\varepsilon(\phi(\mathbf{y})) d\mathbf{y}}{\int K_\sigma(\mathbf{x} - \mathbf{y}) H_\varepsilon(\phi(\mathbf{y})) d\mathbf{y}} \\ &= \frac{K_\sigma(\mathbf{x}) * [I^2(\mathbf{x}) H_\varepsilon(\phi(\mathbf{x}))]}{K_\sigma(\mathbf{x}) * H_\varepsilon(\phi(\mathbf{x}))} - \frac{2u_1(\mathbf{x}) \{K_\sigma(\mathbf{x}) * [I(\mathbf{x}) H_\varepsilon(\phi(\mathbf{x}))]\}}{K_\sigma(\mathbf{x}) * H_\varepsilon(\phi(\mathbf{x}))} + \frac{u_1^2(\mathbf{x}) [K_\sigma(\mathbf{x}) * H_\varepsilon(\phi(\mathbf{x}))]}{K_\sigma(\mathbf{x}) * H_\varepsilon(\phi(\mathbf{x}))}, \\ \sigma_2^2(\mathbf{x}) &= \frac{K_\sigma(\mathbf{x}) * [I^2(\mathbf{x})(1 - H_\varepsilon(\phi(\mathbf{x})))]}{K_\sigma(\mathbf{x}) * (1 - H_\varepsilon(\phi(\mathbf{x})))} - \frac{2u_2(\mathbf{x}) \{K_\sigma(\mathbf{x}) * [I(\mathbf{x})(1 - H_\varepsilon(\phi(\mathbf{x})))]\}}{K_\sigma(\mathbf{x}) * (1 - H_\varepsilon(\phi(\mathbf{x})))} + \frac{u_2^2(\mathbf{x}) [K_\sigma(\mathbf{x}) * (1 - H_\varepsilon(\phi(\mathbf{x})))]}{K_\sigma(\mathbf{x}) * (1 - H_\varepsilon(\phi(\mathbf{x})))}.\end{aligned}$$

Then  $e_1$  and  $e_2$  are calculated as follows:

$$e_i = K_\sigma(\mathbf{x}) * \log \sigma_i(\mathbf{x}) + \frac{1}{2} I^2(\mathbf{x}) \left[ K_\sigma(\mathbf{x}) * \left( \frac{1}{\sigma_i^2(\mathbf{x})} \right) \right] - I(\mathbf{x}) \left[ K_\sigma(\mathbf{x}) * \left( \frac{u_i(\mathbf{x})}{\sigma_i^2(\mathbf{x})} \right) \right] + \frac{1}{2} \left[ K_\sigma(\mathbf{x}) * \left( \frac{u_i^2(\mathbf{x})}{\sigma_i^2(\mathbf{x})} \right) \right], \quad i = 1, 2.$$

Secondly, we can use the analogical process to describe the calculations of the global means  $u_3(\mathbf{x})$ ,  $u_4(\mathbf{x})$ , variances  $\sigma_3^2(\mathbf{x})$ ,  $\sigma_4^2(\mathbf{x})$ ,  $e_3$  and  $e_4$ .

Note that it is unnecessary to reinitialize the level set function due to the introduction of DRLSE. For its excellent effect on maintaining the regularity and stability, as described in [25,41,42,45], we can initialize the level set function as follows:

$$\phi_0(\mathbf{x}) = \begin{cases} a, & \mathbf{x} \in \Omega_0 \\ -a, & \text{otherwise} \end{cases} \quad (27)$$

where  $\Omega_0 \subset \Omega$ , and  $a$  is a positive constant. Furthermore, we use a simple finite difference explicit scheme to discretize the level set formulation (24) as follows:

$$\frac{\phi^{n+1} - \phi^n}{\Delta t} = \mu \operatorname{div}(d_p(|\nabla \phi^n|) \nabla \phi^n) + \nu \delta_\varepsilon(\phi^n) \operatorname{div} \left( \frac{\nabla \phi^n}{|\nabla \phi^n|} \right) - \delta_\varepsilon(\phi^n) [(1 - \theta)(e_1 - e_2) + \theta(e_3 - e_4)], \quad (28)$$

where we take into account the Neumann boundary condition.

Next, a direct implementation of the proposed active contour model is presented in Algorithm 1.

**Algorithm 1.** The implementation of the proposed active contour model: fixed weighting coefficient  $\theta$  and time step  $\Delta t$

---

Input:  $I$ .  
Initialize:  $\phi^0 = \phi_0(\mathbf{x})$ ,  $\mu$ ,  $\nu$ ,  $\varepsilon$ ,  $\sigma$ .  
Choose:  $\theta$ ,  $\Delta t$ .  
 $n = 1$ .  
**while** the solution is not converged **do**  
  Compute  $u_1(\mathbf{x})$ ,  $u_2(\mathbf{x})$ ,  $\sigma_1^2(\mathbf{x})$ ,  $\sigma_2^2(\mathbf{x})$  by using Eqs. (16)–(19) sequentially.  
  Compute  $u_3$ ,  $u_4$ ,  $\sigma_3^2$ ,  $\sigma_4^2$  by using Eqs. (20)–(23) sequentially.  
  Update level set function  $\phi^{n+1}$  by solving level set formulation (24).  
   $n = n + 1$ .  
**end while**

---

**Remark 2.** In Algorithm 1, the choice of  $\theta$  relies on the degree of the intensity inhomogeneity of the image.

In practice, as we have pointed out above, it is necessary to choose a suitable weighting coefficient  $\theta$  to better balance the local and global region fitting energies for image segmentation. Moreover, to some extent, apart from the cooperation, both of them exist with mutual competition. For example, setting a large  $\theta$  for the image with severe intensity inhomogeneity, such as magnetic resonance (MR) image may lead to undesirable results. The reason is that the global region fitting energy plays a leading role under this condition. On the other hand, if  $\theta$  is too small, the proposed model is with slow convergence and sensitive to the initialization of the contour. As a special case, it may get stuck in local minima and fail in extracting the desired objects far away from the initial contour. What is more, in terms of actual applications, sometimes we only need to obtain some selective objects rather than overall ones, so we try to set a small  $\theta$  and initialize the contour near the desired object at this moment. Actually, it is illogical and improper to always set a small  $\theta$  because sometimes initializing the contour near the desired object is not an easy task, especially for the image with multiple objects or a complex background. In addition, even to a common image, selecting a suitable constant  $\theta$  needs a great number of trials and modifications and the process is time-consuming.

Considering the existing problem about the choice of the weighting coefficient, we further present a modified algorithm in which the weighting coefficient  $\theta$  and the time step  $\Delta t$  can be adaptively changed with the contour evolution. In other words, they are not always two fixed constants. For simplicity, we can set a relatively large  $\theta$  and a relatively large  $\Delta t$  for the benefit of initializing the contour and speeding up the convergence rate at the beginning. Then when the contour goes near the object boundaries, we reduce  $\theta$  gradually in order to decrease the weight of the global region fitting energy and increase the weight of the local region fitting energy. Meanwhile, if it is necessary, we reduce  $\Delta t$  to decrease the convergence rate for the benefit of detecting the object boundaries accurately. Specifically, the main idea and procedure are described as in [Algorithm 2](#).

**Algorithm 2.** The implementation of the proposed active contour model: changing weighting coefficient  $\theta$  and time step  $\Delta t$

---

Input:  $I$ .  
Initialize:  $\phi^0 = \phi_0(\mathbf{x}), \mu, \nu, \varepsilon, \sigma, T_1, T_2, T_3, T_4$ .  
Compute:  $[M, N] = \text{size}(I)$ .  
Choose:  $\theta, \Delta t$ .  
 $n = 1$ .  
**while** the solution is not converged **do**  
  Compute  $u_1(\mathbf{x}), u_2(\mathbf{x}), \sigma_1^2(\mathbf{x}), \sigma_2^2(\mathbf{x})$  by using Eqs. (16)–(19) sequentially.  
  Compute  $u_3, u_4, \sigma_3^2, \sigma_4^2$  by using Eqs. (20)–(23) sequentially.  
   $c = 0, L = 0$ .  
  **for**  $i = 1$  to  $M$  **do**  
    **for**  $j = 1$  to  $N$  **do**  
      **if**  $|\phi^n(i, j)| \leq T_1$  **and**  $|\nabla I(i, j)| \geq T_2$  **then**  
         $c = c + 1$ .  
        **if**  $c \geq T_3$  **then**  
           $\theta = \theta/2$ .  
          **if**  $\Delta t \geq T_4$  **then**  
             $\Delta t = \Delta t/2$ .  
          **end if**  
           $L = 1$ , break.  
        **end if**  
      **end if**  
    **end for**  
  **if**  $L == 1$  **then**  
    break.  
  **end if**  
  **end for**  
  Update level set function  $\phi^{n+1}$  by solving level set formulation (24).  
   $n = n + 1$ . **end while**

---

**Remark 3.** In [Algorithm 2](#), we first need to access the size of the image  $I$  by  $[M, N] = \text{size}(I)$ , where  $M$  is the height and  $N$  is the width.  $c$  is a counter for counting pixels.  $T_1, T_2, T_3$  and  $T_4$  are preset threshold constants. Considering the level set function and the image with the same domain, we adopt the index  $(i, j)$  to find the relation between  $\phi(i, j)$  and  $I(i, j)$ . More specifically, in every iteration, all the points on the level set surface and all the pixels of the image are used to realize the loop. For each index  $(i, j)$ , if the corresponding point on the level set surface meets  $|\phi^n(i, j)| \leq T_1$ , then this point is considered to be close to the present zero level set. On this basis, for the same index  $(i, j)$ , if the corresponding pixel of the image meets  $|\nabla I(i, j)| \geq T_2$ , which means the position of this pixel with high gradient, then  $c = c + 1$ . Generally speaking, the gradient of the object boundary of the image is always high. Further if  $c \geq T_3$ , it means these pixels with high gradients are enough, and consequently we deduce that the present zero level set is close to object boundaries. In other words, the contour  $C$  is near the object boundaries, then we have  $\theta = \theta/2$ . to decrease the weight of the global region fitting energy and increase the weight of the local region fitting energy. Meanwhile, if  $\Delta t \geq T_4$ , then  $\Delta t = \Delta t/2$ .  $L$  is a flag to be used to judge whether we have reduced  $\theta$  because it is permitted to change once in each iteration.

**Remark 4.** In [Algorithm 2](#), the choices of the four threshold constants  $T_1, T_2, T_3$  and  $T_4$  are very important to improve the segmentation quality and reduce the iteration time. In general,  $T_1$  should be relatively small for it is used to deduce whether the point on the level set surface is near the present zero level set. Based on the same index  $(i, j)$ ,  $T_2$  is used to judge whether the corresponding pixel of the image is in or near the high gradient areas.  $T_3$  is used to judge whether these pixels are enough, which should be relatively large in order to avoid mistaking due to the interference of noise.  $T_4$  is used to judge whether it is necessary to continually reduce  $\Delta t$ .



**Remark 5.** In Algorithm 2,  $|\nabla I(i,j)| = \sqrt{I_x^2(i,j) + I_y^2(i,j)}$ , where  $I_x(i,j)$  and  $I_y(i,j)$  are calculated by using the central difference scheme in the interior points and the forward or backward difference scheme on the boundary points.

In Algorithm 2, by employing the value of the level set function and the gradient information of the image, we mainly focus on judging whether the contour  $C$  is close to the object boundaries. Generally, we consider when the zero level set is near the high gradient areas, which means that the contour  $C$  is close to the object boundaries. Therefore, we decrease the weighting coefficient  $\theta$ , which signifies changing the weight between the local and global region fitting energies. From Algorithm 2, we can obtain an adaptive weighting coefficient  $\theta$  and a fit time step  $\Delta t$ , which are helpful to detect the object boundaries accurately and reduce the iteration time. Besides, as far as we are concerned, it can deal with the problem of the initialization for different requirements. To be specific, we can select a relatively large weighting coefficient  $\theta$  at the beginning.

#### 4. Experimental results and discussions

In this section, a series of synthetical and real-world images are used to test the effectiveness and performance of the proposed active contour model and its corresponding algorithms. All the experiments are mainly divided into two categories for respectively verifying Algorithms 1 and 2, which are implemented in Matlab 7.0 on a personal computer with Inter Pentium CPU 2.80 GHz and 4 GB of memory. Unless otherwise specified, the default parameters are set as  $a = 2$ ,  $\mu = 0.04$ ,  $v = 0.00001 \times 255^2$ ,  $\varepsilon = 1.0$ ,  $\sigma = 3.0$ ,  $\Delta t = 1.0$ ,  $T_1 = 0.1$ ,  $T_2 = 4.0$ ,  $T_3 = 10$ ,  $T_4 = 0.2$ . In the following experiments, the choice of the weighting coefficient  $\theta$  mainly depends on the degree of the intensity inhomogeneity of the image.

##### 4.1. Experiments for Algorithm 1

In the beginning, we test the effectiveness of Algorithm 1. As discussed in Section 3.2, it is very critical for Algorithm 1 to set a suitable weighting coefficient  $\theta$  to balance the weight between the local and global region fitting energies. Fig. 1 shows the comparison results of the C-V model and Algorithm 1 on a synthetic image with blurred boundaries. We use two kinds of the initialization as in Fig. 1(a) and (d). Fig. 1(b) and (e) are the results of the C-V model which are accurate and desirable. With the same initial contours, Algorithm 1 can achieve similar results as in Fig. 1(c) and (f), where we choose  $\theta = 0.8$  owing to the image with low intensity inhomogeneity. From the comparison results we can see that the effectiveness is similar between the C-V model and Algorithm 1.

Fig. 2 shows a comparison on the C-V model, the LBF model and Algorithm 1 for a synthetical image and two X-ray images. All of them are typical images with intensity inhomogeneity [23]. The first column presents the initial contours. The second column shows the results of the C-V model in which partial objects and backgrounds are mixed with each other. These results clearly demonstrate that the C-V model cannot handle the intensity inhomogeneity well as explained in Section 2.1. The third and fourth columns are the results of the LBF model and Algorithm 1, respectively, and both of them are similar. Due to these images with intensity inhomogeneity, we choose  $\theta = 0.01$  in the first row,  $\theta = 0.05$  in the second row

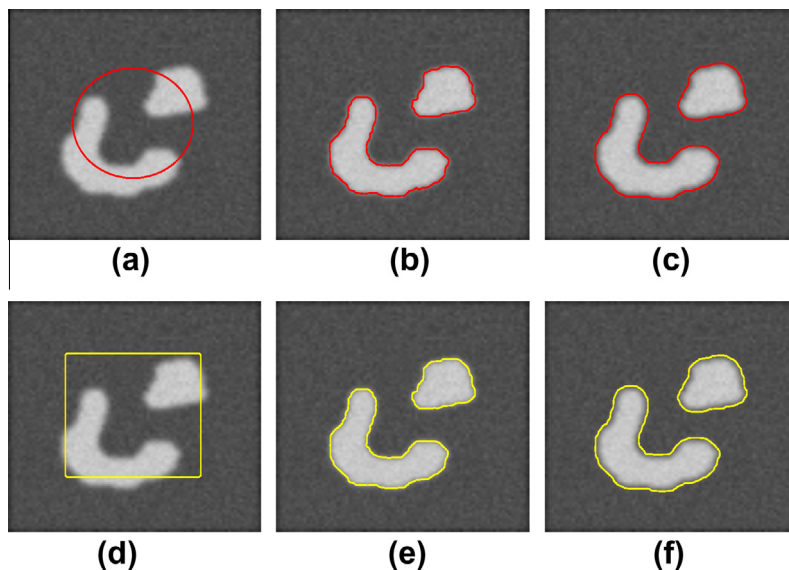


**Fig. 1.** Comparison results for a synthetic image. (a) and (d) are initial contours. (b) and (e) are the results of the C-V model. (c) and (f) are the results of Algorithm 1.

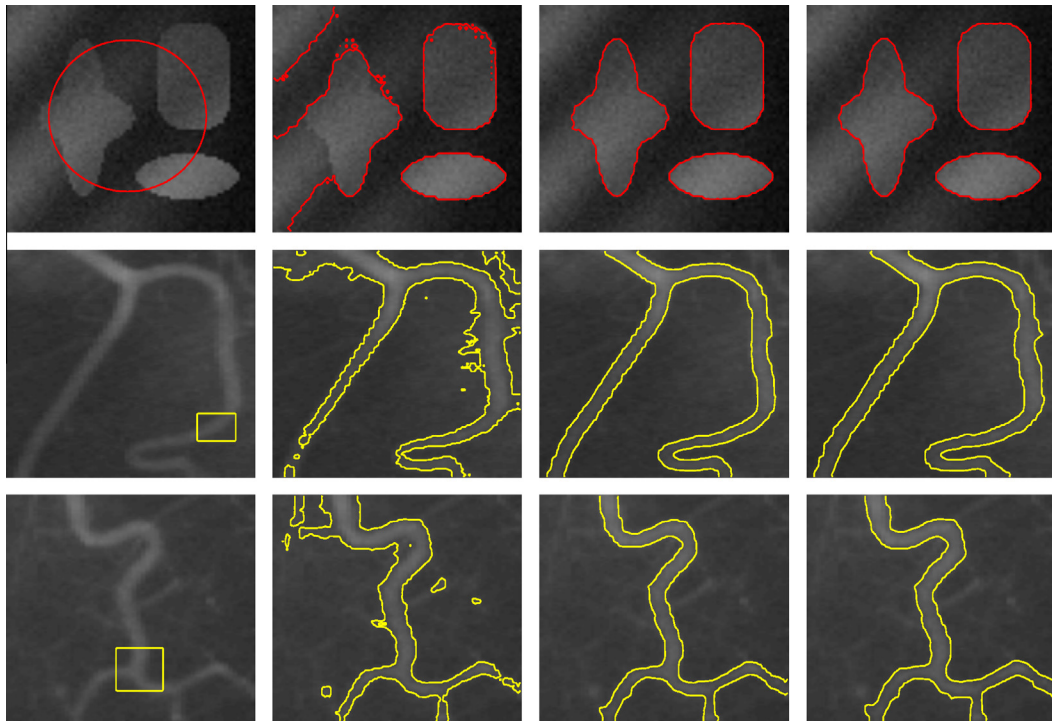


**Fig. 2.** Comparison results for images with intensity inhomogeneity. Column 1: initial contours. Column 2: results of the C-V model. Column 3: results of the LBF model. Column 4: results of [Algorithm 1](#).

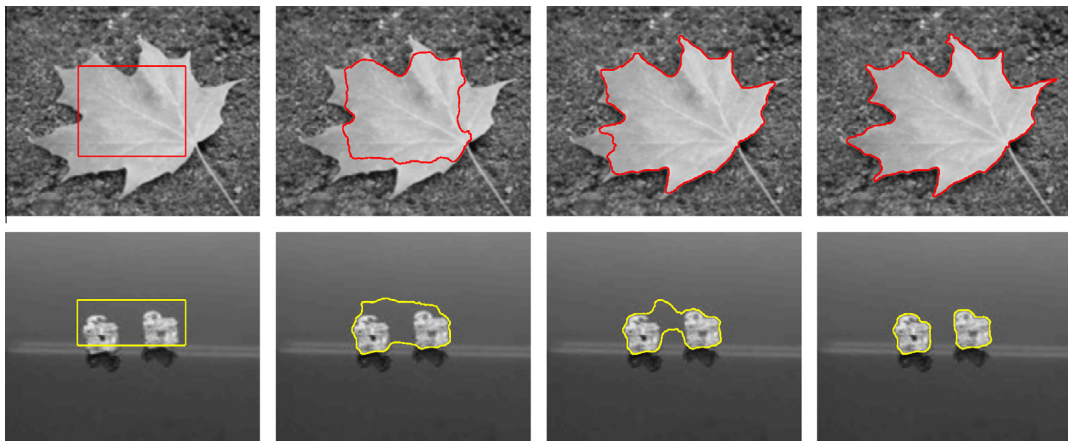


**Fig. 3.** Results of [Algorithm 1](#) with application to two real-world images. Column 1: initial contours. Column 2 and Column 3: intermediate results. Column 4: final results.

and  $\theta = 0.05$ ,  $\nu = 0.000015 \times 255^2$  in the third row. These experiment results illustrate that our algorithm can obtain satisfactory results by choosing a suitable weighting coefficient  $\theta$ , like the LBF model.

[Fig. 3](#) demonstrates the effectiveness of [Algorithm 1](#) with application to real-world images. Every row is the initial contour, intermediate results and the final result from left to right. The process of the contour evolution indicates that the contour is driven by the local and global region fitting energies and gradually moves toward the object boundaries. We choose  $\theta = 0.2$  and  $\nu = 0.00002 \times 255^2$ .

Next, we test the performance of [Algorithm 1](#) on some synthetic images with noise in [Fig. 4](#). We set the different locations for initial contours. [Fig. 4\(a\)](#) and [\(g\)](#) show that the initial contours intersect with the objects and backgrounds. [Fig. 4\(b\)](#) and [\(h\)](#) are the corresponding results. [Fig. 4\(c\)](#) shows that the initial contour is completely inside the object and [Fig. 4\(d\)](#) is the final result. [Fig. 4\(e\)](#) shows that the initial contour is fully outside the object and the final result is shown in [Fig. 4\(f\)](#). [Fig. 4](#)

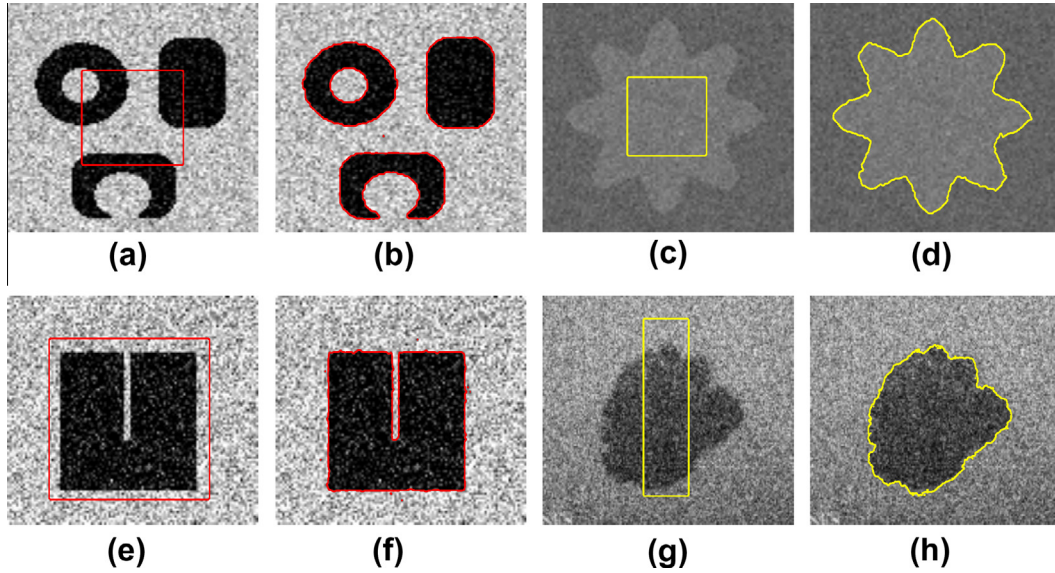


**Fig. 4.** Results for synthetic images with noise. (a), (c), (e) and (g) are initial contours. (b), (d), (f) and (h) are the results of Algorithm 1.

indicates that Algorithm 1 is less sensitive to the noise and the initialization of the contour. We choose  $\theta = 0.5$  and  $\nu = 0.00002 \times 255^2$ .

#### 4.2. Experiments for Algorithm 2

As described and analyzed in Section 3.2, sometimes selecting a suitable constant  $\theta$  for Algorithm 1 requires many trials and this process is time-consuming. Therefore, we further present Algorithm 2 in which we can obtain an adaptive  $\theta$  and a fit  $\Delta t$  with the contour evolution. In particular, for the image with intensity inhomogeneity, when the initial contour is far away from the object boundaries, choosing a relatively large or small constant  $\theta$  is not suitable for Algorithm 1. In practice, according to Algorithm 2, it is appropriate to follow a flexible way that we choose a relatively large  $\theta$  and a relatively large  $\Delta t$  at the beginning and gradually decrease them when the contour goes near the object boundaries. In the following experiments, we concentrate on demonstrating the effectiveness and performance of Algorithm 2.

Fig. 5 shows some comparisons of the performance between the LBF model and Algorithm 2 on medical images with intensity inhomogeneity. As a matter of fact, it is significant about how to extract the desired objects for medical images. Every row presents the initial contour, the result of the LBF model and the result of Algorithm 2 from left to right. In the first row, an X-ray image of the vessel is tested and the final results of two methods are similar. Nevertheless, for the ultrasound image in the second row and especially the MR image with a tumor in the third row, it is clear that the performance of Algorithm 2 is better than the LBF model. We choose  $\theta = 1.0$ ,  $T_4 = 1.0$  in the first row,  $\theta = 0.1$ ,  $\nu = 0.00002 \times 255^2$  in the second row and  $\theta = 0.1$ ,  $\nu = 0.000026 \times 255^2$ ,  $T_4 = 1.0$  in the third row. Furthermore, Fig. 5 also demonstrates that Algorithm 2 is effective to extract the desired objects. Specifically, the comparison iterations of convergence and CPU time in seconds corresponding to Fig. 5 are listed in Table 1, which show that Algorithm 2 takes more iterations and CPU time than the LBF model. In fact, according to the discussion in Section 3.2, it is reasonable for our algorithm to be of more computational complexity.

In order to specify the change of the weighting coefficient, Fig. 6 shows three examples to illustrate the effectiveness of Algorithm 2. The first and second rows exhibit the images with intensity inhomogeneity, where we choose  $\theta = 1.0$ ,  $\nu = 0.000035 \times 255^2$ ,  $T_2 = 6.0$  and  $\theta = 1.0$ ,  $\nu = 0.00004 \times 255^2$ ,  $T_1 = 0.3$ ,  $T_4 = 1.0$ , respectively. The third row is a microscope image of cells where we choose  $\theta = 1.0$ ,  $\nu = 0.000032 \times 255^2$ . The first column presents the initial contours and the second column shows the intermediate results. The third column is the final results. According to Algorithm 2, when the contour goes near the object boundaries, the weighting coefficient  $\theta$  and the time step  $\Delta t$  will correspondingly decrease. The fourth column is the changing curves of  $\theta$  and  $\Delta t$  for the first 50 iterations. From the curves we can observe that  $\theta$  and  $\Delta t$  remain unchanged at the beginning and then gradually reduce with the increasing iterations. After 50 iterations,  $\theta$  approaches to zero which indicates that the dominant fitting energy of the proposed model has shifted from the global region fitting energy to the local region fitting energy. Furthermore, reducing  $\theta$  and  $\Delta t$  is beneficial to accurately detect the object boundaries. And especially for the concave boundaries in Fig. 6(b) and the fuzzy boundaries in Fig. 6(k), Algorithm 2 performs very well.

From the viewpoint of the content and structure, even though Algorithm 2 is more complex than Algorithms 1, and 1 is sensitive to the choice of the initial contour. That is to say, an unfit initialization may lead to slow convergence or

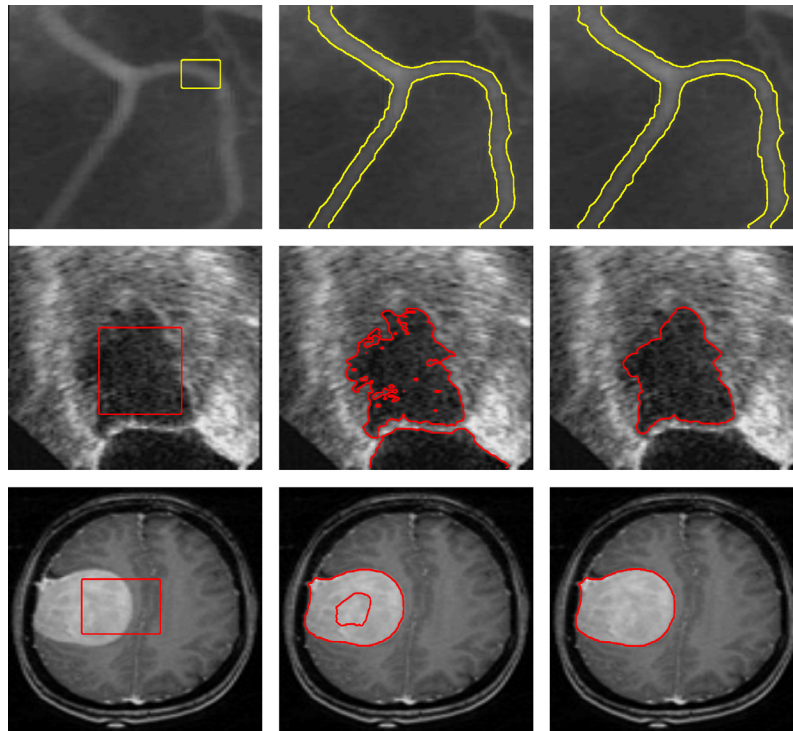


**Fig. 5.** Comparison results for medical images. Column 1: initial contours. Column 2: results of the LBF model. Column 3: results of Algorithm 2.

**Table 1**

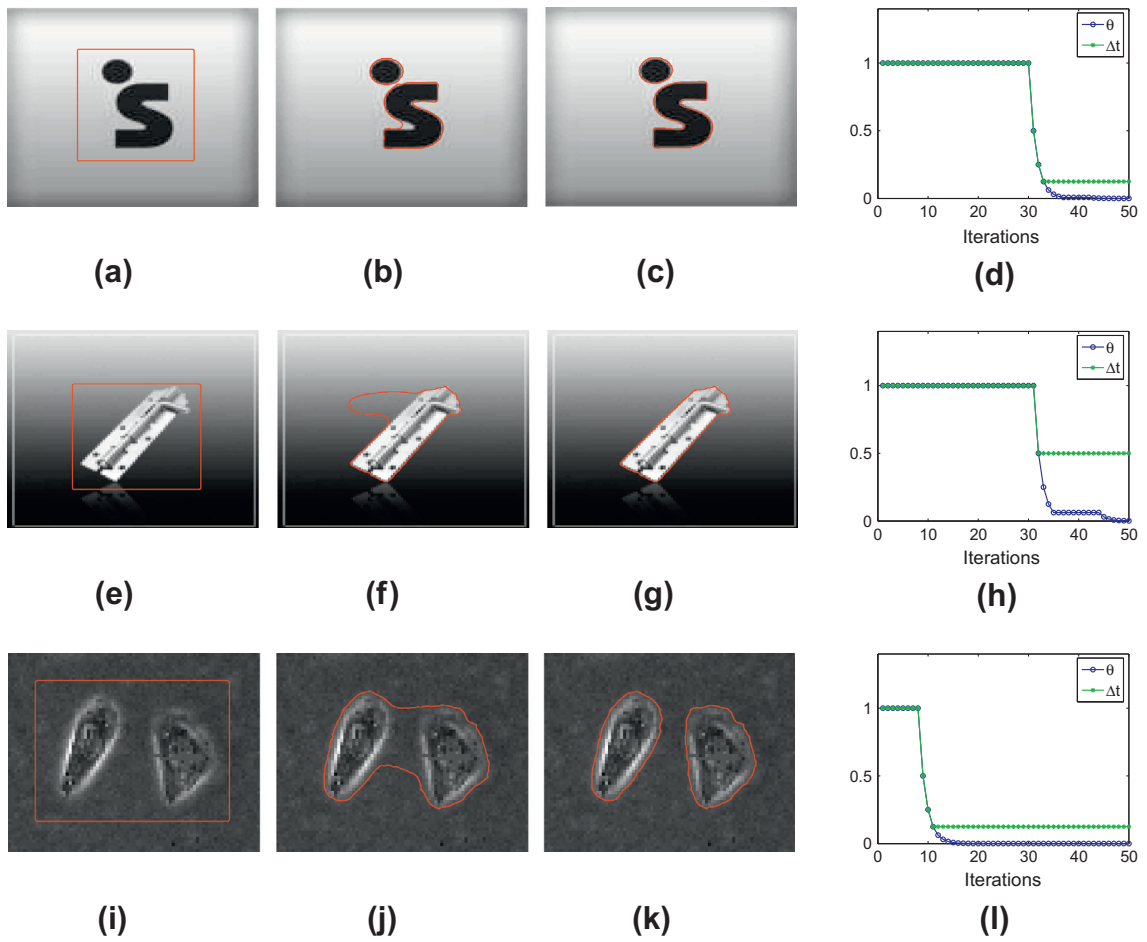
Iterations and CPU time of the experiment in Fig. 5.

	LBF [22,23]		Algorithm 2	
	Iterations	Time (s)	Iterations	Time (s)
Vessel image	400	8.94	1500	85.08
Ultrasound image	300	5.87	2000	81.49
MR image	500	10.22	1400	74.61

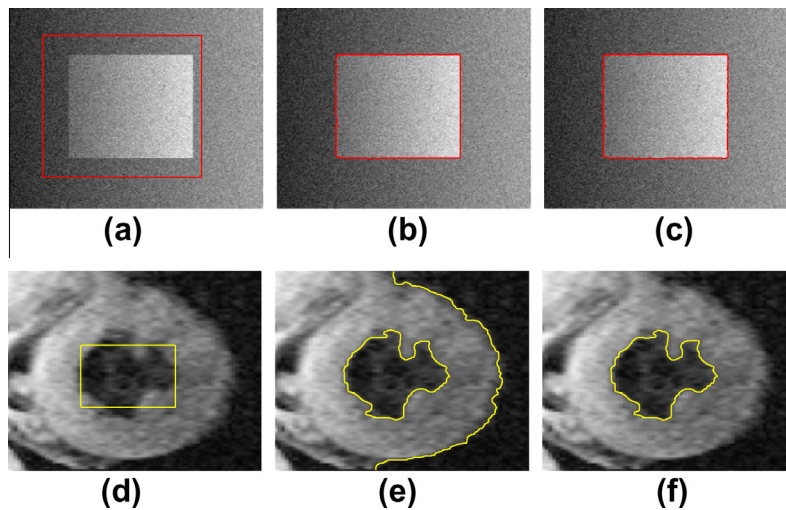
dissatisfactory results. Besides, in order to speed up the convergence rate for Algorithm 2, we can choose a relatively large  $\theta$ . Fig. 7 indicates the relationship between Algorithms 1 and 2 based on the same initial conditions. The first row is a synthetic image with noise and its size is  $206 \times 195$  pixels. Fig. 7(a) is the initial contour. Fig. 7(b) is the result of Algorithm 1 where  $\theta = 0.01$ ,  $\nu = 0.00002 \times 255^2$ . Fig. 7(c) is the result of Algorithm 2 where  $\theta = 1.0$ ,  $\nu = 0.00002 \times 255^2$ ,  $T_1 = 0.01$ ,  $T_2 = 6.0$ ,  $T_3 = 20$ ,  $T_4 = 1.0$ . The second row is a MR image and its size is  $136 \times 132$  pixels. Fig. 7(d) is the initial contour. Fig. 7(e) is the result of Algorithm 1 where  $\theta = 0.2$ ,  $\nu = 0.00002 \times 255^2$ . This result seems not to be desirable for all the boundaries are detected completely. Fig. 7(f) is the result of Algorithm 2 where  $\theta = 1.0$ ,  $\nu = 0.00002 \times 255^2$ ,  $T_1 = 0.05$ ,  $T_4 = 0.5$ . Here, we obtain the desired result. As discussed in Section 3.2, when the contour goes near object boundaries,  $\theta$  becomes smaller and smaller with the contour evolution. In fact, the global region fitting energy is dominant at the beginning and the local region fitting energy plays a leading role after some iterations. These experiment results illustrate that Algorithm 2 is flexible to extract the desired objects. The comparison iterations of convergence and CPU time for Fig. 7 are listed in Table 2, from which we can clearly observe that Algorithm 2 with fewer iterations and less CPU time is faster than Algorithm 1.

For validating the effectiveness of Algorithm 2 on the image with intensity inhomogeneity, a series of synthetic images have been tested and the corresponding results are shown in Fig. 8. Fig. 8(a) is the initial contour and Fig. 8(b) is the result, where  $\theta = 0.1$ ,  $\nu = 0.00003 \times 255^2$ ,  $T_4 = 1.0$ . Fig. 8(c) is the initial contour and Fig. 8(d) is the result, where  $\theta = 0.5$ ,  $\nu = 0.000038 \times 255^2$ ,  $T_4 = 0.5$ . Fig. 8(e) is the initial contour and Fig. 8(f) is the result, where  $\theta = 0.6$ ,  $\nu = 0.00003 \times 255^2$ ,  $T_4 = 0.5$ . Fig. 8(g) is the initial contour and Fig. 8(h) is the result, where  $\theta = 1.0$ ,  $\nu = 0.00003 \times 255^2$ . These experiment results verify that the effectiveness of Algorithm 2 is satisfying when applied to the synthetic images with intensity inhomogeneity.





**Fig. 6.** Results and curves. (a), (e) and (i) are initial contours. (b), (f) and (j) are the intermediate results of Algorithm 2. (c), (g) and (k) are the final results of Algorithm 2. (d), (h) and (l) are the changing curves of  $\theta$  and  $\Delta t$  for the first 50 iterations.

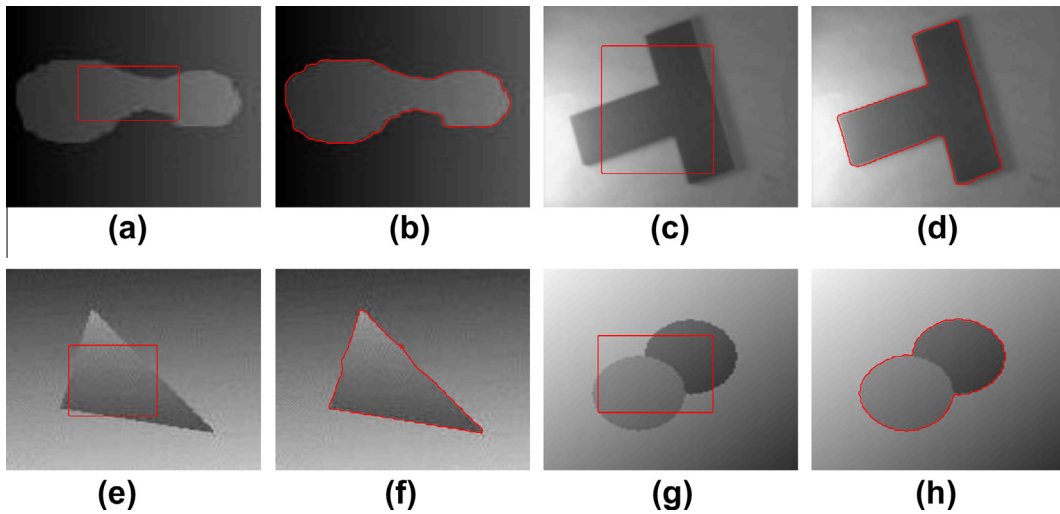
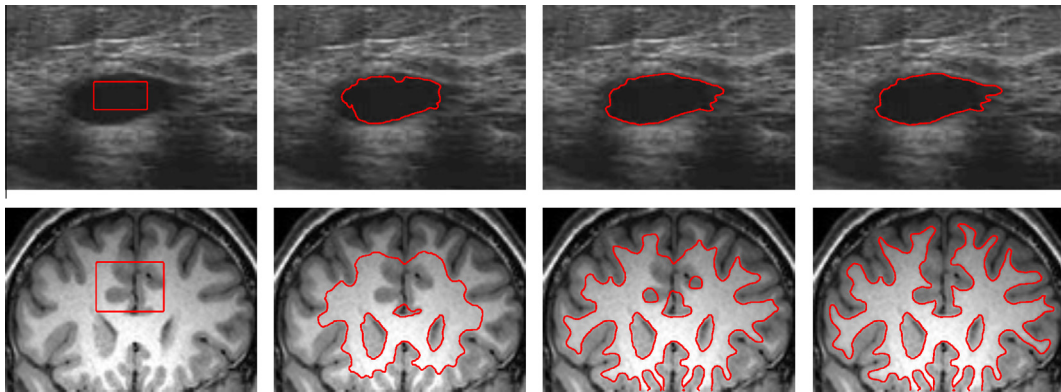


**Fig. 7.** Comparison results of two algorithms. (a) and (d) are initial contours. (b) and (e) are the results of Algorithm 1. (c) and (f) are the results of Algorithm 2.

**Table 2**

Iterations and CPU time of the experiment in Fig. 7.

	Algorithm 1		Algorithm 2	
	Iterations	Time (s)	Iterations	Time (s)
Synthetical image	1150	190.51	650	108.33
MR image	1200	86.69	1000	72.18

**Fig. 8.** Results for synthetic images with intensity inhomogeneity. (a), (c), (e) and (g) are initial contours. (b), (d), (f) and (h) are the results of Algorithm 2.**Fig. 9.** Results for Algorithm 2 with application to medical images. Column 1: initial contours. Column 2 and Column 3: intermediate results. Column 4: final results.

Subsequently, a further experiment is carried out to test the effectiveness of Algorithm 2 on medical images again and its results are shown in Fig. 9. We choose an ultrasound image in the first row and a brain MR image in the second row. Every row is the initial contour, intermediate results and the final result. Here, taking account of the convergence rate, we choose  $\theta = 1.0$  for the ultrasound image and the object boundaries are detected well. Similarly, for the brain MR image, we set  $\theta = 1.0$ ,  $T_1 = 0.01$ ,  $T_4 = 1.0$ . The result manifests that almost all white matter is successfully extracted. The iterations of convergence and CPU time for Fig. 9 are shown in Table 3.

At last, we focus on demonstrating the effectiveness of Algorithm 2 on a synthetic image with the noise and intensity inhomogeneity as in Fig. 10. Fig. 10(a) and (e) are two different initial contours. Fig. 10(b) and (f) are the results of interactive active contour (IAC) [33] model, where the performance is not desirable. As described in [33], the IAC model is mainly an integration of geodesic active contour (GAC) model [9] and the C-V model. Because of incorporating the edge information and the global region information, without involving the local region information, it is unable to deal with the problem of



**Table 3**  
Iterations and CPU time of the experiment in Fig. 9.

	Iterations	Time (s)
Ultrasound image	800	40.21
MR image	900	39.09

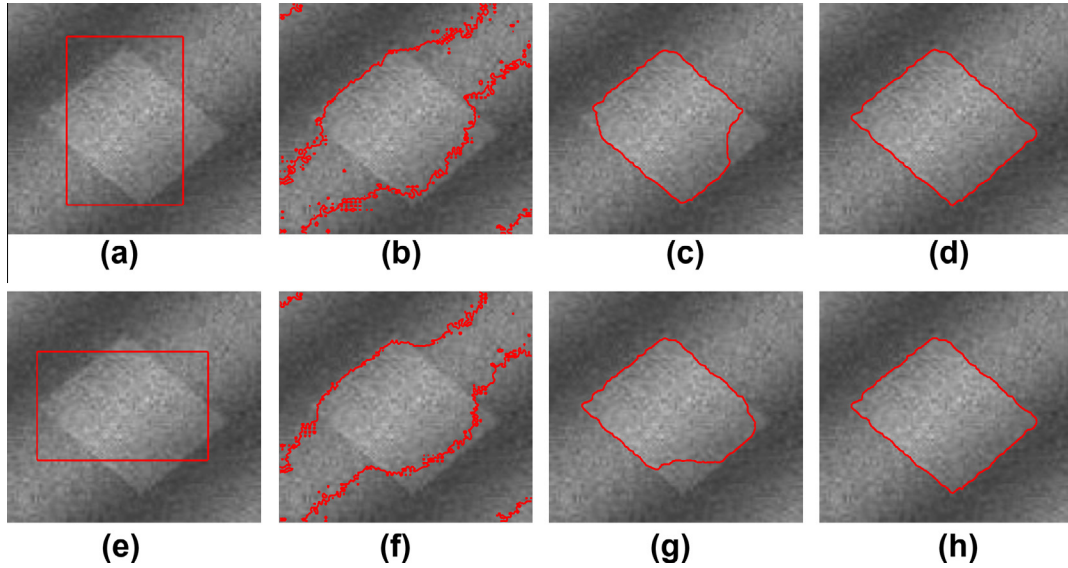


**Fig. 10.** Comparison results for a synthetic image with noise and intensity inhomogeneity. (a) and (e) are initial contours. (b) and (f) are the results of the IAC model [33]. (c) and (g) are the results of Wang et al. [42]. (d) and (h) are the results of Algorithm 2.

**Table 4**  
Iterations and CPU time of the comparison experiment in Fig. 10.

	IAC [33]		Wang et al. [42]		Algorithm 2	
	Iterations	Time (s)	Iterations	Time (s)	Iterations	Time (s)
Row 1	150	5.16	1500	30.62	1500	84.45
Row 2	150	3.87	1500	30.55	1500	84.38

the intensity inhomogeneity well. Fig. 10(c) and (g) are the results of Wang et al. [42] which is a direct combination of the C-V model and the LBF model. Fig. 10(d) and (h) are the results of Algorithm 2. These experiment results demonstrate that Algorithm 2 is robust to the presence of the noise and intensity inhomogeneity. In our algorithm, the weighting coefficient and the time step can be dynamically changed with the alteration of the contour location, which is more flexible than the model in [42]. We set  $\theta = 0.1$ ,  $\nu = 0.00003 \times 255^2$ ,  $T_1 = 0.02$ ,  $T_4 = 1.0$ . The comparison iterations of convergence and CPU time for Fig. 10 are listed in Table 4, which illustrates that our algorithm takes more computational time. Even so, our algorithm is very flexible and effective.

#### 4.3. Discussion on parameters

In Sections 4.1 and 4.2, according to different experiment images, we choose different parameters. Like other related methods, the choices of parameters are essential to improve the quality of segmentation. In Algorithm 1, the selection of the weighting coefficient  $\theta$  relies on the degree of the intensity inhomogeneity of the image. But for Algorithm 2, it is relatively convenient. In fact, as shown in Section 4.2, in most cases, we choose  $\theta = 1.0$  because its value will be adaptively changed with the level set evolution. Here, we mainly focus on discussing the parameters  $T_1$ ,  $T_2$ ,  $T_3$  and  $T_4$ , which play a significant role to obtain satisfactory results. Generally,  $T_1$  should be small.  $T_2$  should be large because it is a threshold of the gradient module. Especially to the image with strong noise, it is reasonable to be relatively large. For the image with weak or fuzzy boundaries, it should be small.  $T_3$  is a threshold of the counter. For the image with many high gradient areas, it should be large. For the image with clear object boundaries and a simple background, it can be chosen as a small value.  $T_4$  is a threshold to be used to judge whether it is necessary to reduce the time step. For the image with complex object bound-

aries, we should set it to be small so that the time step is continuously reduced for the benefit of detecting the boundaries accurately. On the other hand, if it is too small, the time step may become smaller and smaller, which will impact the speed of our algorithm, and especially increase the computational cost. Based on a lot of tests and our experience, we have  $T_1 \in [0, 0.5]$ ,  $T_2 \in [2, 10]$ ,  $T_3 \in [8, 20]$  and  $T_4 \in [0.1, 1.0]$ .

## 5. Conclusion

In this paper, an active contour model and its corresponding algorithms with local and global Gaussian distribution fitting energies have been proposed for image segmentation. First of all, based on the advantages of the local and global region fitting energies, we proposed an active contour model which incorporates both the local and global region information of the image. In this proposed model, we increased the weighting coefficient to combine the local and global region fitting energies which are described by the local and global Gaussian distributions with different means and variances, respectively. Subsequently, an algorithm has been presented for implementing the proposed model directly, in which the effectiveness mainly depends on the choice of the weighting coefficient under certain conditions. Generally, for the image with low intensity inhomogeneity, this algorithm is satisfactory. However, in practice, selecting a suitable weighting coefficient may be difficult and time-consuming. To overcome this problem, we further presented a modified algorithm which can obtain an adaptive weighting coefficient and a fit time step with the contour evolution. In our algorithm, we can choose a relatively large weighting coefficient at the beginning, then it will decrease when the contour goes near the object boundaries. This algorithm is less sensitive to the initialization of the contour and can speed up the convergence rate. Furthermore, it is flexible to change the weight between the local and global region fitting energies, which is beneficial and significant to improve the quality of segmentation. Therefore, it is effective for the image with intensity inhomogeneity. In addition, it is robust to the noise and can be used to extract the desired objects. In the future work, we will proceed to extend the proposed model and its corresponding algorithms to the color image segmentation [11,44] and the applications to tracking [26,47].

## Acknowledgments

The authors would like to thank the editor-in-chief Prof. Witold Pedrycz and anonymous referees for their valuable comments and suggestions, which are very helpful for revising and improving this paper. This research is supported by 973 Program (2013CB329404), NSFC (61170311, 61370147, 11201054), Sichuan Province Sci. & Tech. Research Project (2012GZX0080), and the Fundamental Research Funds for the Central Universities (09CX04003A).

## References

- [1] I.B. Ayed, N. Hennane, A. Mitiche, Unsupervised variational image segmentation/classification using a Weibull observation model, *IEEE Transactions on Image Processing* 15 (11) (2006) 3431–3439.
- [2] I.B. Ayed, A. Mitiche, Z. Belhadj, Multiregion level-set partitioning of synthetic aperture radar images, *IEEE Transactions on Pattern Analysis and Machine Intelligence* 27 (5) (2005) 793–800.
- [3] N. Badshah, K. Chen, Image selective segmentation under geometrical constraints using an active contour approach, *Communications in Computational Physics* 7 (4) (2010) 759–778.
- [4] J.M. Beaulieu, R. Touzi, Segmentation of textured polarimetric SAR scenes by likelihood approximation, *IEEE Transactions on Geoscience and Remote Sensing* 42 (10) (2004) 2063–2072.
- [5] D. Boukerroui, A. Baskurt, J.A. Noble, O. Basset, Segmentation of ultrasound images-multiresolution 2-D and 3-D algorithm based on global and local statistics, *Pattern Recognition Letters* 24 (4–5) (2003) 779–790.
- [6] X. Bresson, S. Esedoglu, P. Vanderghynst, J.-P. Thiran, S. Osher, Fast global minimization of the active contour/snake model, *Journal of Mathematical Imaging and Vision* 28 (2) (2007) 151–167.
- [7] E.S. Brown, T.F. Chan, X. Bresson, Completely convex formulation of the Chan-Vese image segmentation model, *International Journal of Computer Vision* 98 (1) (2012) 103–121.
- [8] V. Caselles, F. Catte, T. Coll, F. Dibos, A geometric model for active contours in image processing, *Numerische Mathematik* 66 (1) (1993) 1–31.
- [9] V. Caselles, R. Kimmel, G. Sapiro, Geodesic active contours, *International Journal of Computer Vision* 22 (1) (1997) 61–79.
- [10] T.F. Chan, S. Esedoglu, M. Nikolova, Algorithms for finding global minimizers of image segmentation and denoising models, *SIAM Journal on Applied Mathematics* 66 (5) (2006) 1632–1648.
- [11] T.F. Chan, B.Y. Sandberg, L.A. Vese, Active contours without edges for vector-valued images, *Journal of Visual Communication and Image Representation* 11 (2) (2000) 130–141.
- [12] T.F. Chan, L.A. Vese, Active contours without edges, *IEEE Transactions on Image Processing* 10 (2) (2001) 266–277.
- [13] D. Cremers, M. Rousson, R. Deriche, A review of statistical approaches to level set segmentation: integrating color, texture, motion and shape, *International Journal of Computer Vision* 72 (2) (2007) 195–215.
- [14] V. Estellers, D. Zosso, R. Lai, S. Osher, J.-P. Thiran, X. Bresson, Efficient algorithm for level set method preserving distance function, *IEEE Transactions on Image Processing* 21 (12) (2012) 4722–4734.
- [15] R. Goldenberg, R. Kimmel, E. Rivlin, M. Rudzsky, Fast geodesic active contours, *IEEE Transactions on Image Processing* 10 (10) (2001) 1467–1475.
- [16] J. Ghasemi, R. Ghaderi, M.R. Karami Mollaei, S.A. Hojjatoleslami, A novel fuzzy Dempster-Shafer inference system for brain MRI segmentation, *Information Sciences* 223 (20) (2013) 205–220.
- [17] J. Gomes, O. Faugeras, Reconciling distance functions and level sets, *Journal of Visual Communication and Image Representation* 11 (2) (2000) 209–223.
- [18] J. Huang, X. Yang, Y. Chen, A fast algorithm for global minimization of maximum likelihood based on ultrasound image segmentation, *Inverse Problems and Imaging* 5 (3) (2011) 645–657.
- [19] M. Kass, A. Witkin, D. Terzopoulos, Snakes: active contour models, *International Journal of Computer Vision* 1 (4) (1988) 321–331.
- [20] J. Kim, J.W. Fisher, A. Yezzi, M. Cetin, A.S. Willsky, A nonparametric statistical method for image segmentation using information theory and curve evolution, *IEEE Transactions on Image Processing* 14 (10) (2005) 1486–1502.
- [21] S. Lankton, A. Tannenbaum, Localizing region-based active contours, *IEEE Transactions on Image Processing* 17 (11) (2008) 2029–2039.

- [22] C. Li, C. Kao, J.C. Gore, Z. Ding, Implicit active contours driven by local binary fitting energy, in: *Proceedings of IEEE Conference on Computer Vision and Pattern Recognition*, Minneapolis, 2007, pp. 1–7.
- [23] C. Li, C. Kao, J.C. Gore, Z. Ding, Minimization of region-scalable fitting energy for image segmentation, *IEEE Transactions on Image Processing* 17 (10) (2008) 1940–1949.
- [24] C. Li, C. Xu, C. Gui, M.D. Fox, Level set evolution without re-initialization: a new variational formulation, in: *Proceedings of IEEE Conference on Computer Vision and Pattern Recognition*, San Diego, 2005, pp. 430–436.
- [25] C. Li, C. Xu, C. Gui, M.D. Fox, Distance regularized level set evolution and its application to image segmentation, *IEEE Transactions on Image Processing* 19 (12) (2010) 3243–3254.
- [26] H. Liu, F. Sun, Efficient visual tracking using particle filter with incremental likelihood calculation, *Information Sciences* 195 (15) (2012) 141–153.
- [27] A. Mitiche, I.B. Ayed, *Variational and Level Set Methods in Image Segmentation*, Springer, New York, 2010.
- [28] D. Mumford, J. Shah, Optimal approximations by piecewise smooth functions and associated variational problems, *Communications on Pure and Applied Mathematics* 42 (5) (1989) 577–685.
- [29] S. Osher, J.A. Sethian, Fronts propagating with curvature-dependent speed: algorithms based on Hamilton–Jacobi formulation, *Journal of Computational Physics* 79 (1) (1988) 12–49.
- [30] J. Park, J.M. Keller, Snakes on the watershed, *IEEE Transactions on Pattern Analysis and Machine Intelligence* 23 (10) (2001) 1201–1205.
- [31] I. Posirca, Y. Chen, C.Z. Barcelos, A new stochastic variational PDE model for soft Mumford–Shah segmentation, *Journal of Mathematical Analysis and Applications* 384 (1) (2011) 104–114.
- [32] L. Rada, K. Chen, A new variational model with dual level set functions for selective segmentation, *Communications in Computational Physics* 12 (1) (2012) 261–283.
- [33] C. Sagiv, N.A. Sochen, Y.Y. Zeevi, Integrated active contours for texture segmentation, *IEEE Transactions on Image Processing* 15 (6) (2006) 1633–1646.
- [34] C. Samson, L. Blanc-Feraud, G. Aubert, J. Zerubia, A level set model for image classification, *International Journal of Computer Vision* 40 (3) (2000) 187–197.
- [35] A. Sarti, C. Corsi, E. Mazzini, C. Lamberti, Maximum likelihood segmentation of ultrasound images with Rayleigh distribution, *IEEE Transactions on Ultrasonics, Ferroelectrics, and Frequency Control* 52 (6) (2005) 947–960.
- [36] D. Sen, S.K. Pal, Improving feature space based image segmentation via density modification, *Information Sciences* 191 (15) (2012) 69–191.
- [37] M. Sussman, P. Smereka, S. Osher, A level set approach for computing solutions to incompressible two-phase flow, *Journal of Computational Physics* 114 (1) (1994) 146–159.
- [38] A. Tsai, A. Yezzi, A.S. Willsky, Curve evolution implementation of the Mumford–Shah functional for image segmentation, denoising, interpolation, and magnification, *IEEE Transactions on Image Processing* 10 (8) (2001) 1169–1186.
- [39] A. Vasilievskiy, K. Siddiqi, Flux-maximizing geometric flows, *IEEE Transactions on Pattern Analysis and Machine Intelligence* 24 (12) (2002) 1565–1578.
- [40] L.A. Vese, T.F. Chan, A multiphase level set framework for image segmentation using the Mumford and Shah model, *International Journal of Computer Vision* 50 (3) (2002) 271–293.
- [41] L. Wang, L. He, A. Mishra, C. Li, Active contours driven by local Gaussian distribution fitting energy, *Signal Processing* 89 (12) (2009) 2435–2447.
- [42] L. Wang, C. Li, Q. Sun, D. Xia, C. Kao, Active contours driven by local and global intensity fitting energy with application to brain MR image segmentation, *Computerized Medical Imaging and Graphics* 33 (7) (2009) 520–531.
- [43] Y. Xiang, A. Chung, J. Ye, An active contour model for image segmentation based on elastic interaction, *Journal of Computational Physics* 219 (1) (2006) 455–476.
- [44] X.D. Yue, D.Q. Miao, N. Zhang, L.B. Cao, Q. Wu, Multiscale roughness measure for color image segmentation, *Information Sciences* 216 (20) (2012) 93–112.
- [45] K. Zhang, H. Song, L. Zhang, Active contours driven by local image fitting energy, *Pattern Recognition* 43 (4) (2010) 1199–1206.
- [46] K. Zhang, L. Zhang, H. Song, W. Zhou, Active contours with selective local or global segmentation: a new formulation and level set method, *Image and Vision Computing* 28 (4) (2010) 668–676.
- [47] S. Zheng, An intensive restraint topology adaptive snake model and its application in tracking dynamic image sequence, *Information Sciences* 180 (16) (2010) 2940–2959.
- [48] S.C. Zhu, A. Yuille, Region competition: unifying snakes, region growing, and Bayes/MDL for multiband image segmentation, *IEEE Transactions on Pattern Analysis and Machine Intelligence* 18 (9) (1996) 884–900.